# Supplementary Information

# Thermal evolution of solid solution of silica embedded AgPt alloy NPs in the large miscibility gap

Hemant Jatav[1], Anusmita Chakravorty[1,2], Ambuj Mishra[1], Matthias Schwartzkopf[3], Andrei Chumakov[3], Stephan V. Roth[3,4] and Debdulal Kabiraj[1*] (✉)

[1] *Materials science department, Inter-University Accelerator Centre, Aruna Asaf Ali Marg, New Delhi, 110067, India*

[2] *The Pennsylvania State university, University Park, PA, 16802, USA*

[3] *Deutsches Elektronen-Synchrotron (DESY), Notkestraße 85, D-22607 Hamburg, Germany*

[4] *KTH Royal Institute of Technology, Department of Fibre and Polymer Technology, Teknikringen 56-58,*

*SE-100 44 Stockholm, Sweden*

*Corresponding Author\*: Dr. Debdulal Kabiraj (d.kabiraj@gmail.com)*

**Synthesis:** The nanocomposite (NC) thin films consisting of metal nanoparticles (NPs) inside the silica matrix were prepared using Atom Beam Sputtering (ABS) technique. The detailed information about the setup and operating conditions are reported in our previous paper [1]. The composition of the elements was controlled by the sputtering rate and the relative area exposed to the 600 eV neutral Argon atom beam. For $AgPt/SiO_2$ NCs, four foils of Pt and Ag each, with an optimized surface area were pasted to a quartz target (3-inch diameter), and then all three components (Metal, Si, and O) were co-sputtered under high vacuum in an ABS chamber to prepare the desired thin-films on the Si and quartz substrate. The surface area of each metal foil used for deposition was $5 \times 5$ mm$^2$. Due to its optical transparency, quartz substrate was selected for UV-Visible absorption spectroscopy measurements, while silicon substrate was used for all other characterizations.

**Rutherford Backscattering spectrometry (RBS):** RBS measurement was performed to evaluate the film thickness and relative metal concentration of $AgPt/SiO_2$ NC. The film thickness of $(295 \pm 15)$ nm is observed for pristine sample.
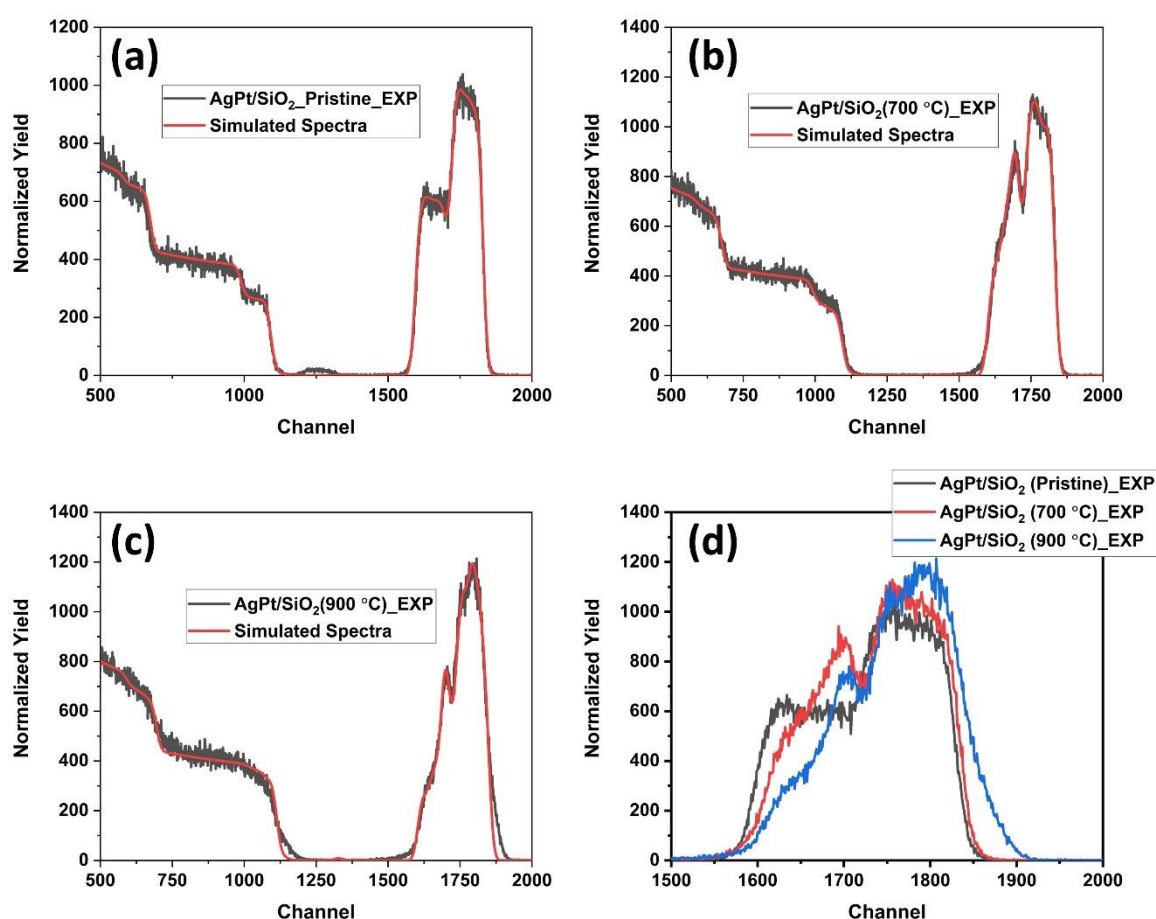


**Figure S1** RBS spectra of $AgPt/SiO_2$ NC thin film for (a) as-deposited (pristine) (b) 700 ℃, and (c) 900 ℃ annealed samples. Here red solid line shows the fitted spectra simulated using Rutherford Universal Manipulation Program (RUMP) [2]. (d) Comparison of Ag and Pt backscattered signals at indicated ATs for understanding the temperature-dependent diffusion of Ag and Pt atoms within the silica matrix.

It can be seen from Fig S1d that the elemental peak of Ag is gradually shifting towards the higher channel number, indicating the diffusion of Ag atoms towards the surface of the NC thin films with increase in annealing temperature. Further quantification using rump simulation reveal that the Ag concentration inside the silica matrix is reduced by 47% for 900 ℃ annealed sample in comparison to as-deposited sample. Whereas almost 20% reduction in Ag concentration is observed for 700 ℃ annealed sample in comparison to as-deposited sample.

**X-ray photoelectron spectroscopy (XPS):**

XPS is an effective and sensitive technique for determining changes in the chemical state of any element at the surface (~5-10 nm). Shirley background correction is used to filter out in-elastically scattered background photoelectrons. To fit the experimental spectra, Lorentzian asymmetric line shape is used. The 3d spectrum of Ag component in $Ag/SiO_2$ is composed of four peaks (FIG S2(b)). First two peaks, peak1 (367 eV) and peak2 (372.8 eV) are due to the spin-orbital splitting of Ag 3d orbital into 3d5/2 and Ag 3d3/2 respectively. These assigned peaks and their positions are in good agreement with previously reported data. Other two satellite peaks near 369.5 eV and 375 eV are may be due to the presence of Ag ions. Absence of any peak at higher binding energy (BE) along with pure Ag(0) peak, denying the formation of Ag oxides. Fig. S2(d) shows the XPS spectra of Pt component of $Pt/SiO_2$ NC. For the corresponding BE values of 316.2 eV and 333.2 eV, peaks are identified as Pt 4d5/2 and Pt 4d3/2, respectively. Similar to Ag, other two satellite peaks are also observed.

In case of bimetallic NPs, Ag 3d component of $AgPt/SiO_2$ also have four components as shown in FIG S2(a), First two peaks, peak1 (368.2 eV) and peak2 (374 eV) are due to the spin-orbital splitting of Ag 3d orbital into 3d5/2 and Ag 3d3/2 respectively. Other two satellite peaks near 370 eV and 377 eV may be occurred due to the presence of Ag ions, resulting from the charge exchange between metals due to alloying. No signature of oxidation state is observed. Fig. S2(c) shows the XPS spectra of Pt component of $AgPt/SiO_2$ NC. For the corresponding BE values of 316 eV and 333 eV, peaks are identified as Pt 4d5/2 and Pt 4d3/2, respectively. Similar to Ag, other two satellite peaks are also observed. The pure state of Ag NPs with no oxidation is also confirmed by HRTEM images. It is observed that a negative shift of 0.2 eV in the B.E. is observed for Pt 4d component of $AgPt/SiO_2$ NC with respect to $Pt/SiO_2$ NC and a large positive shift of 1.2 eV is observed for Ag 3d component of $AgPt/SiO_2$ NC with respect to $Ag/SiO_2$ NC.
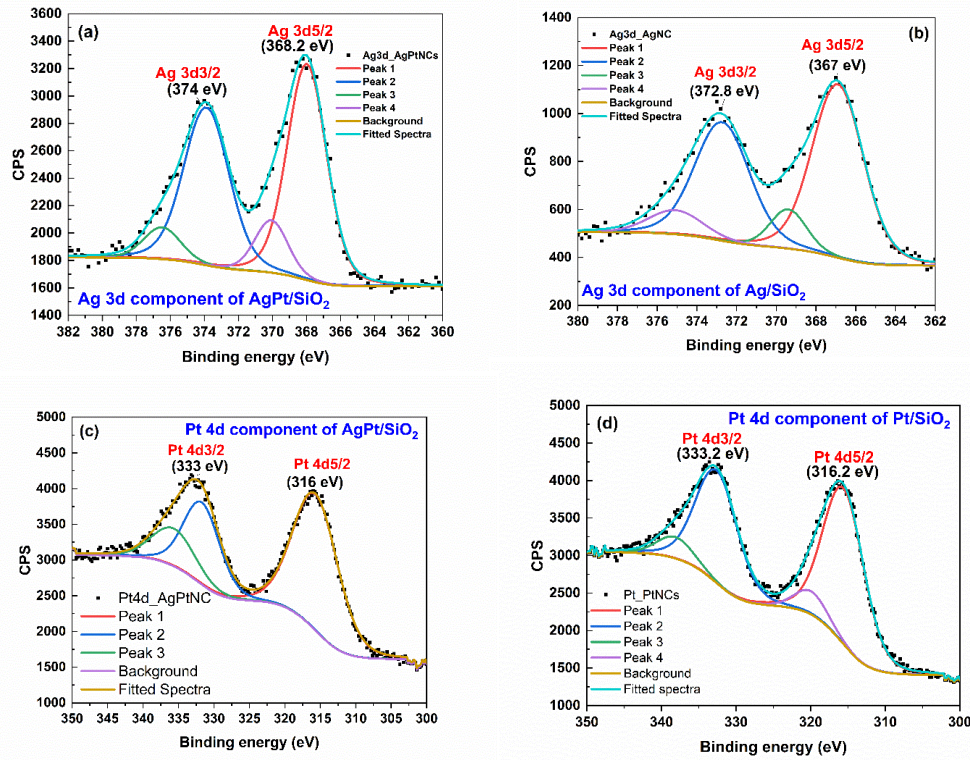
**Figure S2.** The core-level XPS spectra of the Ag component of the (a) AgPt/SiO₂ NC and (b) Ag/SiO₂ NC are presented. Prior to peak fitting, Shirley background has been subtracted from spectrum. For Ag component, four asymmetric Lorentzian peaks were selected to accurately fit the curve. The core-level XPS spectra of the Pt component of the (c) AgPt/SiO₂ NC and (d) Pt/SiO₂ NC are shown. The background correction is performed using the same procedure as followed for the Ag component.

## *In situ* annealing GISAXS/GIWAXS:

The DPDAK software is used to extract the one-dimensional line cuts from the two-dimensional intensity distribution maps of GISAXS [3]. The line cuts in the horizontal (at Yoneda peak position i.e. $q_z = 0.59$ nm$^{-1}$) and vertical directions (at $q_y = 0$ nm$^{-1}$) are shown in the Fig. 5 of the main manuscript. Fig. 5(i) show the position of the Yoneda peak in the vertical cut line profile in terms of critical angle. The position of the Yoneda peak is found at $q_z = 0.59$ nm$^{-1}$ at a critical angle of $\alpha_c = (0.16)°$. FIG. 5(g-h) show the one-dimensional horizontal cut line profile, where a broad scattering peaks are observed, which signifies the presence of well-separated NPs throughout the silica matrix. These peaks are fitted by the Lorentzian function as shown by red color line to evaluate peak position ($q_0$) and peak FWHM. These fitting parameters are related to the maximum interference of scattered waves describing cluster correlation distance ξ, popularly known as inter-particle distance. The quantification of the mean inter-particle distance can be estimated using the fitted mean peak position ($q_0$) as $q_0 \approx 2\pi/\xi$ .
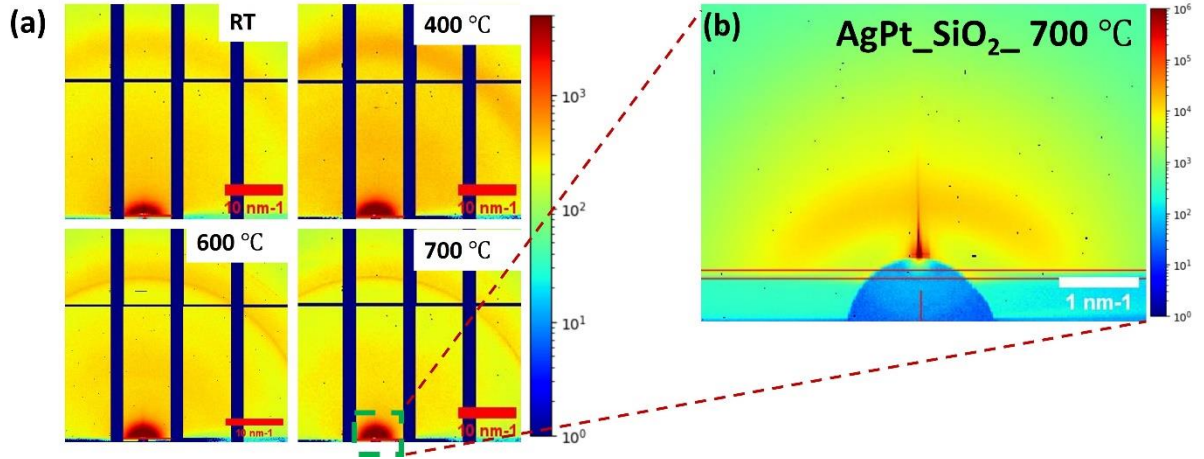
**Figure S3.** The GIWAXS 2D spectrum of (a) AgPt/SiO$_2$ NC are shown at various annealing temperatures taken at the sample-to-dector position of SDD = 206 mm. (b) 2D GIMAXS map extracted from the highlighted region. These enlarged GIMAXS maps were utilized to estimate the size of ultrasmall NPs inside the silica matrix.

For calculating the size of ultra-small AgPt NPs, GIMAXS data was also acquired simultaneously in GIWAXS detector at the sample-to-dector position of SDD = 206 mm. FIG. 5 (c-f) shows the 2D GIMAXS patterns for AgPt-Silica NCs cropped from the GIWAXS data (Fig. S3) at different ATs and their corresponding One-dimensional horizontal cuts were taken at the same critical angle $\alpha_c$ = (0.16)°, and shown in FIG 5(h). To calculate the correlation distance $\xi$, the peaks were fitted using Lorentzian function. 2D GIUSAXS/GIMAXS images show the intensity distribution of scattered signals in the forward direction and a blue dot on the plot shows the specular beams, which are blocked by beam stops to protect the detector from intensity oversaturation.

In horizontal cut graphs (Fig 5(g) and Fig 5(h)), the peak positions are shifting towards the lower $q_y$ values indicates an increase in the inter-particle distance. The change in the inter-particle distances with AT is depicted in Table 1 and 2, shows that the inter-particle distance is increasing with increasing AT. The increase in inter-particle distance indirectly signifies the increase in the mean size of the NPs.

To monitor the growth in size of the NPs inside silica at various ATs, we have utilised the geometrical model of cluster growth proposed by M. Schwartzkopf *et al.* [4]. The model assumes a 2D hexagonal lattice arrangement for spherical metal clusters of radius R with the inter-particle distance $\xi$ between the lattice points. The mean radius of NPs can be evaluated using the knowledge of $\xi$ and the effective thickness ($\delta$) of the silver layer. The mean radius of NPs is calculated using this model, as

$$R = \left[\frac{3^{3/2}}{8\pi}\xi^2\delta\right]^{1/3} \qquad (1)$$

To estimate the effective thickness of the AgPt layer for utilizing the 2D full sphere model, we have considered that our 3D NC thin film is made up of multiple 2D layers stacked on top of each other. In other words, we divide our final NC thickness into slices of 2D layers to calculate the effective layer thickness $\delta$, which is given by

$$\delta = \frac{d_{NC} \times F\%}{\frac{d_{NC}}{\xi} - 1} \qquad (2),$$

here $\delta$ is dependent on the total effective thickness ($d_{NC} = 295 \pm 15$ nm) of 3D NC, metal concentration ($F\% = 0.076 \pm 0.004$) inside the silica matrix and inter-particle distances $\xi$. The calculated values of $\delta$ at various ATs are reported in Table. 1 & 2. The diameter of the NPs are estimated for the left peak positions of the horizontal cut graph using above-mentioned model and the calculated mean diameters of NPs are listed against the AT in Table 1 and 2.

**Grazing-incidence small-angle X-ray scattering:**

**Error propagation analysis**

The uncertainty analysis is calculated using Gaussian error propagation, which is based on the partial differentiation of each independent variables . The uncertainty estimation of peak position ($q_0$) is accurately performed by considering both instrumental ($\Delta q_{y,instr}$) and fitting ($\Delta q_{y,fit}$) errors. Hence, uncertainty in peak position ($q_0$) is calculated by

$$\Delta q_0 = \Delta q_{y,instr} + \Delta q_{y,fit} \qquad \dots\dots\dots\dots. (1),$$

where $\Delta q_{y,fit}$ is the error in mean peak position estimated using Lorentzian fitting and $\Delta q_{y,instr}$ is instrumental error calculated using

$$\Delta q_{y,instr} = \frac{2\pi}{\lambda} \sqrt{\left(\frac{\sin 2\theta_f \, \cos \alpha_f}{\lambda} \Delta\lambda\right)^2 + \left(\sin 2\theta_f \, \sin \alpha_f \, \Delta\alpha_f\right)^2 + \left(\cos 2\theta_f \, \sin \alpha_f \, \Delta 2\theta_f\right)^2} \dots\dots (2)$$

The uncertainty in the different angles $\Delta\alpha_f$ and $\Delta 2\theta_f$ are estimated by detector parameters:

$$\Delta\alpha_f = \sqrt{\left(\frac{s}{D_{SDD}}\Delta Y_{pxl}\right)^2 + \left(\frac{s}{D_{SDD}}\Delta Y_{DB}\right)^2 + \frac{\left(\frac{|Y_{pxl} - Y_{DB}|.s}{D_{SDD}^2}\Delta D_{SDD}\right)^2}{1 + \left(\frac{|Y_{pxl} - Y_{DB}|.s}{D_{SDD}}\right)^2} + \Delta\alpha_i^2} \quad \dots\dots\dots\dots (3)$$

$$\Delta 2\theta_f = \sqrt{\left(\frac{s}{D_{SDD}}\Delta X_{pxl}\right)^2 + \left(\frac{s}{D_{SDD}}\Delta X_{DB}\right)^2 + \frac{\left(\frac{|X_{pxl} - X_{DB}|.s}{D_{SDD}^2}\Delta D_{SDD}\right)^2}{1 + \left(\frac{|X_{pxl} - X_{DB}|.s}{D_{SDD}}\right)^2}} \quad \dots\dots\dots\dots\dots (4),$$

here $s$ represents a pixel size in mm. $D_{SDD}$ is the sample-to-detector distance with uncertainty $\Delta D_{SDD}$. $(X_{pxl}, Y_{pxl})$ denotes an arbitrary position, indicating peak position in the two-dimensional image in X & Y pixel coordinates and their corresponding errors are denoted by $\Delta X_{pxl}$ and $\Delta Y_{pxl}$ respectively. The pixel coordinates of the direct beam in the X and Y directions are denoted by $(X_{DB}, Y_{DB})$ with uncertainty $\Delta X_{DB}$ and $\Delta Y_{DB}$ respectively.

In our calculations, pixel size of $s = 0.172$ mm, sample-to-detector distance $D_{SDD} = 9475 \pm 2$ mm and $\pm 1$ pixel uncertainty for in $X, Y, \Delta X$ and $\Delta Y$ directions for both scattered and direct beams are considered. For horizontal cuts taken from simultaneous acquisition, pixel size of $s = 0.055$ mm, sample-to-detector distance $D_{SDD} = 206 \pm 2$ mm was used. The incident wavelength $\lambda = 0.1048 \pm 0.0008$ nm, incident angle $\alpha_i = \alpha_f = 0.4 \pm 0.002°$ is used as evaluated. The error calculations for inter-particle distances ($\xi$) and effective metal thickness ($\delta$) is calculated by the following formulas and the observed values are listed in table.1.

$$\Delta \xi = \frac{2\pi}{q_0{}^2} \Delta q_0 \qquad \dots\dots\dots\dots\dots\dots\dots\dots. (5)$$

$$\Delta \delta = \sqrt{\left(\frac{\xi^2 \times F\%}{(d_{Nc}-\xi)^2} \Delta d_{NC}\right)^2 + \left(\frac{d_{Nc}{}^2 \times F\%}{(d_{Nc}-\xi)^2} \Delta \xi\right)^2 + \left(\frac{\xi \times d_{Nc}}{(d_{Nc}-\xi)} \Delta F\%\right)^2} \dots\dots\dots\dots\dots\dots (6)$$

**Table. 1**. The peak positions, inter-particle distances, effective thickness and radius of AgPt NPs inside the silica matrix, calculated for the horizontal cuts taken from simultaneous measurement using LAMBDA detector placed at sample-to-detector position of SDD = 206 mm, at the at different annealing temperatures.

| Annealing Temperature ( °C) | Peak position $q_0$ (nm$^{-1}$) | Inter-particle distances (nm) | Effective thickness (nm) | Radius (nm) | Diameter (nm) |
|---|---|---|---|---|---|
| | **Left** | **Left** | **Left** | **Left** | **Left** |
| 25 | $2.12 \pm 0.02$ | $2.96 \pm 0.03$ | $0.23 \pm 0.01$ | $0.74 \pm 0.01$ | $1.48 \pm 0.02$ |
| 400 | $1.96 \pm 0.02$ | $3.21 \pm 0.03$ | $0.25 \pm 0.01$ | $0.81 \pm 0.01$ | $1.62 \pm 0.02$ |
| 600 | $1.86 \pm 0.02$ | $3.38 \pm 0.04$ | $0.26 \pm 0.01$ | $0.85 \pm 0.02$ | $1.70 \pm 0.02$ |
| 700 | $1.73 \pm 0.02$ | $3.63 \pm 0.04$ | $0.28 \pm 0.01$ | $0.91 \pm 0.02$ | $1.82 \pm 0.02$ |

**Table. 2**. The peak positions, inter-particle distances, effective thickness and radius of Ag NPs inside the silica matrix, calculated for the horizontal cuts taken from $GIUSAXS$ measurement using PILATUS detector placed at the sample-to-dector position of SDD = 9475 mm, at different annealing temperatures.

| Annealing Temperature ( °C) | Peak position $q_0$ (nm$^{-1}$) | Inter-particle distances (nm) | Effective thickness (nm) | Radius (nm) | Diameter (nm) |
|---|---|---|---|---|---|
| | **Left** | **Left** | **Left** | **Left** | **Left** |
| 600 | $0.091 \pm 0.001$ | $69.0 \pm 0.6$ | $6.8 \pm 0.4$ | $18.9 \pm 0.4$ | $37.8 \pm 0.8$ |
| 700 | $0.075 \pm 0.001$ | $82.7 \pm 1.1$ | $8.7 \pm 0.5$ | $23.1 \pm 0.5$ | $46.2 \pm 1.0$ |

**Grazing- incidence wide-angle X-ray scattering (GIWAXS):**

The 1D projection of intensity line profile is extracted from 2D GIWAXS diffraction pattern (shown in Fig. S3) using SAXS/WAXS integration module in DPDAK software and plotted in FIG. S4 for AgPt/SiO$_2$, Ag/SiO$_2$, and Pt/SiO$_2$ NCs annealed at 600 ℃. The presence of a major intensity peak around 2θ = 25.96 ± 0.02º and 2θ = 29.94 ± 0.02º confirms the existence of the crystalline Ag and AgPt clusters in the NC thin films. The diffraction angle matches well to the (111) and (200) planes of Ag and AgPt crystal respectively considering the X-ray wavelength of λ = 0.1048 nm [5]. The slight shift in (111) peak position is observed from the bulk Ag, indicating the strain development due to the presence of the surrounding silica matrix. The d-spacing of 0.24 nm calculated from the GIWAXS data is nearly matches with the d-spacing calculated from HRTEM images (Fig. S6).
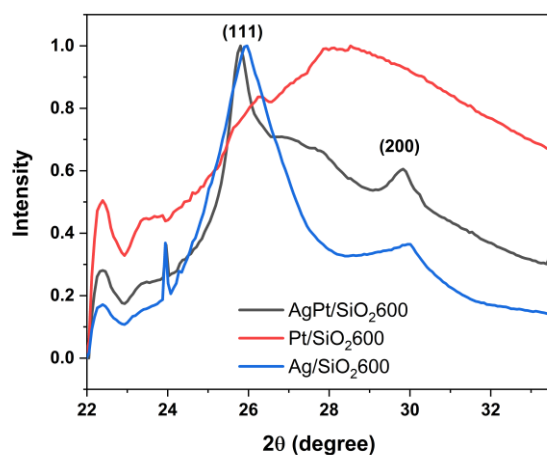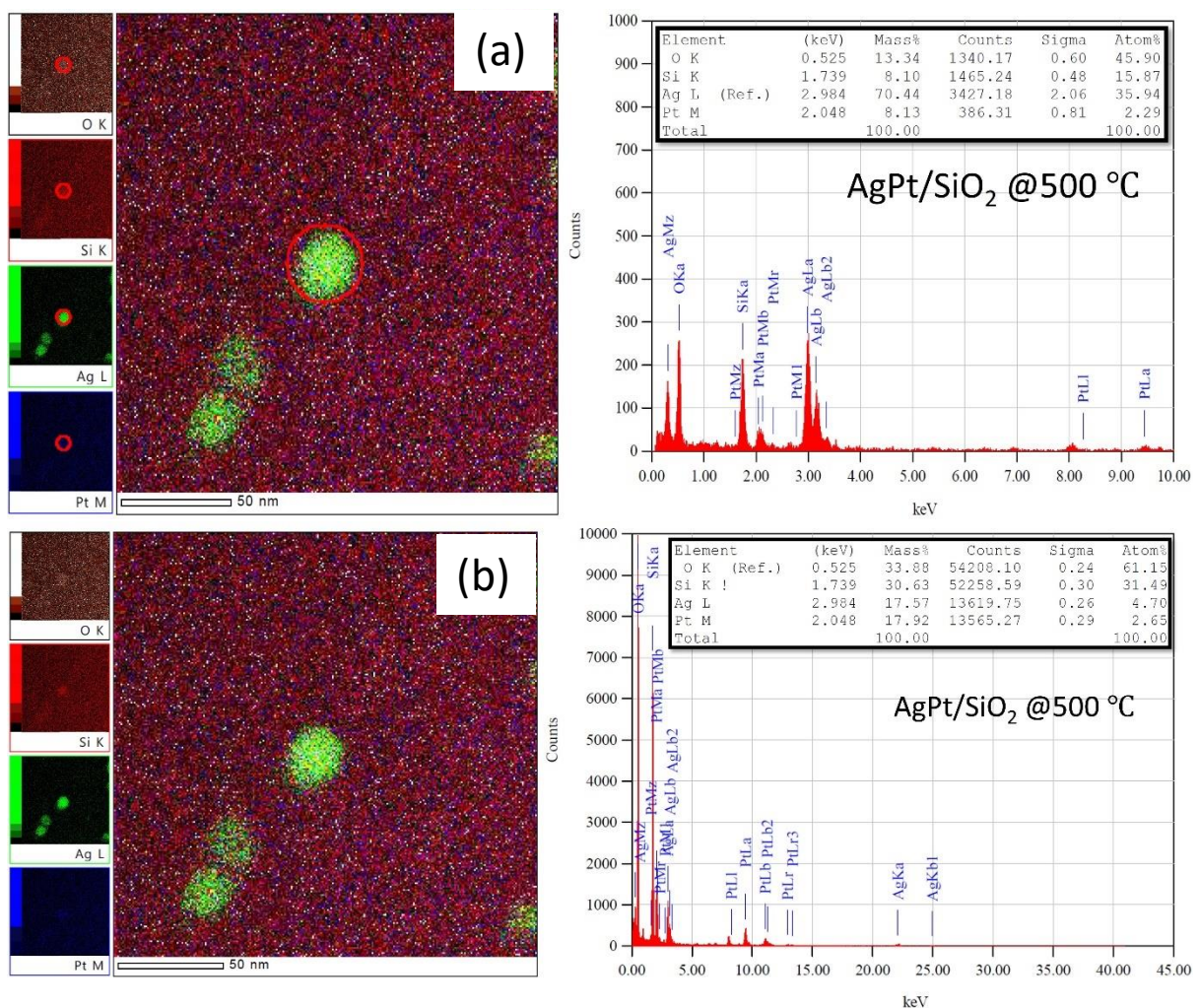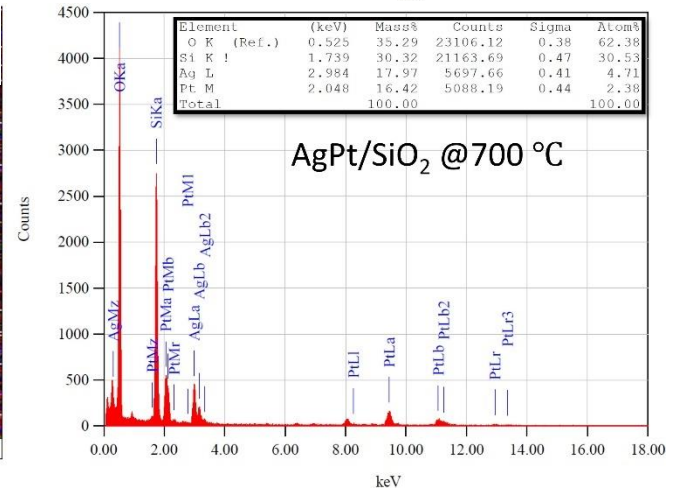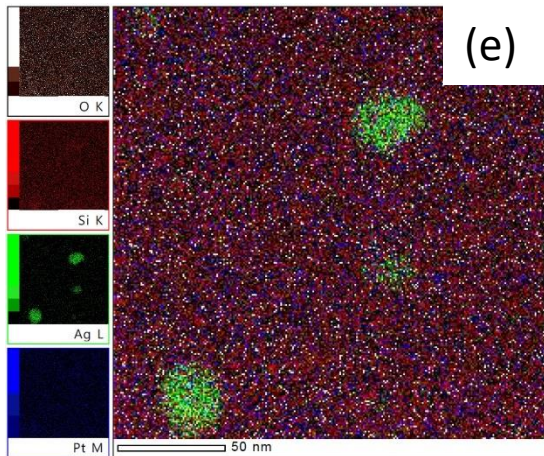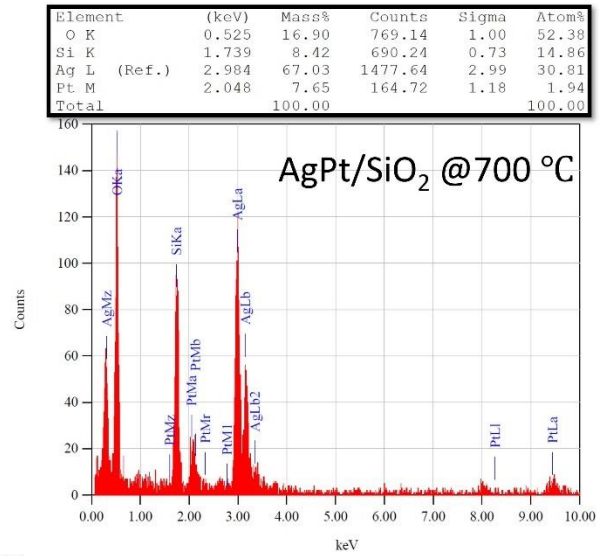


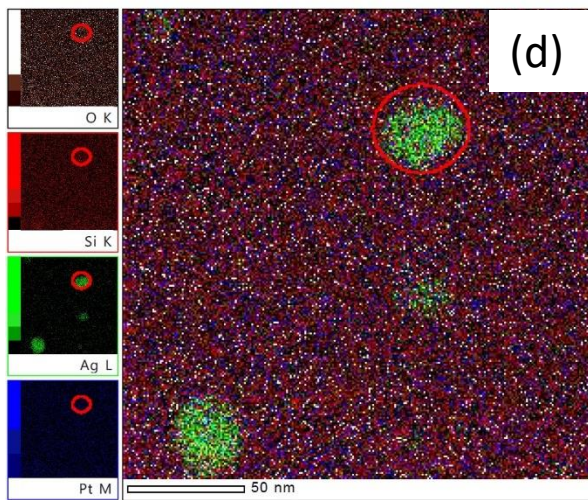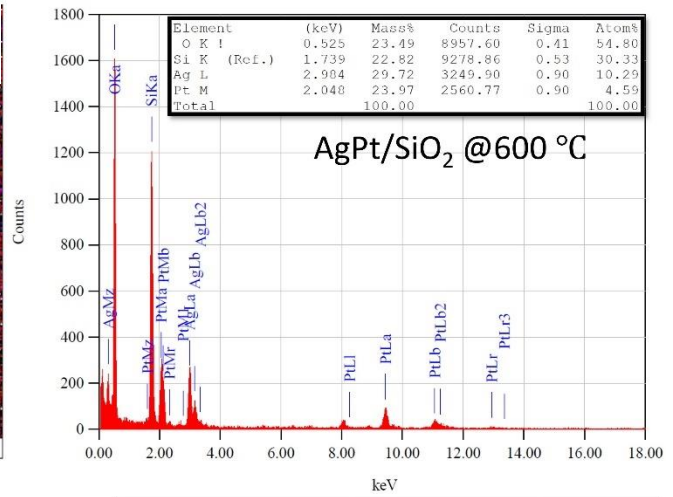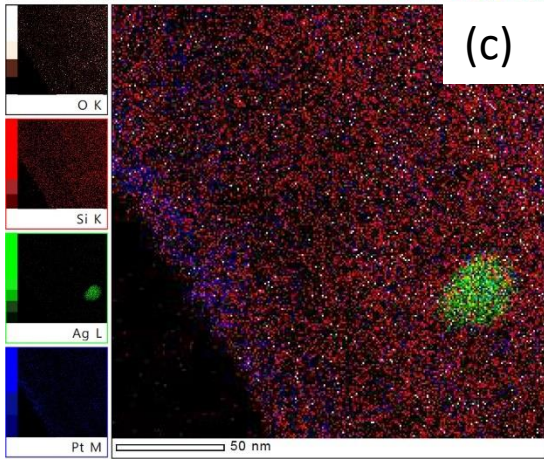**Figure S4.** 1D GIWAXS diffraction pattern extracted from Fig. S3a using SAXS/WAXS integration module in DPDAK software for AgPt/SiO$_2$, Ag/SiO$_2$, and Pt/SiO$_2$ NCs annealed at 600 ℃.

**Transmission Electron Microscopy:**

### (i) Energy dispersive X-ray spectroscopy (EDS) elemental mapping

Energy dispersive X-ray spectroscopy (EDS) maps were acquired in STEM mode for AgPt/SiO$_2$ NC at different annealing temperatures. At 500 ℃, It can be seen that silicon, oxygen, Ag and Pt are uniformly distributed throughout the nanocomposite thin film, indicating the presence of ultrasmall AgPt NPs inside the silica matrix. However, the presence of a few bigger Ag NP is also observed through EDS map and quantification in Fig S5a. Overall, Ag/Pt ratio at 500 ℃ is quantify as 1.77 (Fig S5b), which is quite similar to the RBS quantification. Similar, HAADF-STEM images of AgPt/SiO$_2$ are taken at 600 ℃, 700 ℃ and 900 ℃ and shown in FIG. S5(c-g). The ratio of Ag/Pt is observed to be nearly constant up to the ATs of 700 ℃, However a sharp decline in Ag concentration is observed at 900 ℃. Which signifies the partial emission of Ag atoms from the silica matrix Fig S5(f) and S5(g).



(a)

| Element | | (keV) | Mass% | Counts | Sigma | Atom% |
|---------|---|-------|-------|--------|-------|-------|
| O K | | 0.525 | 13.34 | 1340.17 | 0.60 | 45.90 |
| Si K | | 1.739 | 8.10 | 1465.24 | 0.48 | 15.87 |
| Ag L | (Ref.) | 2.984 | 70.44 | 3427.18 | 2.06 | 35.94 |
| Pt M | | 2.048 | 8.13 | 386.31 | 0.81 | 2.29 |
| Total | | | 100.00 | | | 100.00 |

AgPt/SiO$_2$ @500 ℃



(b)

| Element | | (keV) | Mass% | Counts | Sigma | Atom% |
|---------|---|-------|-------|--------|-------|-------|
| O K | (Ref.) | 0.525 | 33.88 | 54208.10 | 0.24 | 61.15 |
| Si K | ! | 1.739 | 30.63 | 52258.59 | 0.30 | 31.49 |
| Ag L | | 2.984 | 17.57 | 13619.75 | 0.26 | 4.70 |
| Pt M | | 2.048 | 17.92 | 13565.27 | 0.29 | 2.65 |
| Total | | | 100.00 | | | 100.00 |

AgPt/SiO$_2$ @500 ℃

(c)

O K
Si K
Ag L
Pt M

50 nm

| Element | (keV) | Mass% | Counts | Sigma | Atom% |
|---|---|---|---|---|---|
| O K ! | 0.525 | 23.49 | 8957.60 | 0.41 | 54.80 |
| Si K (Ref.) | 1.739 | 22.82 | 9278.86 | 0.53 | 30.33 |
| Ag L | 2.984 | 29.72 | 3249.90 | 0.90 | 10.29 |
| Pt M | 2.048 | 23.97 | 2560.77 | 0.90 | 4.59 |
| Total | | 100.00 | | | 100.00 |

AgPt/SiO$_2$ @600 °C

OKa, AgMz, SiKa, PtMa, PtMb, PtMr, PtMl, AgLa, AgLb, AgLb2, PtLl, PtLa, PtLb, PtLb2, PtLr, PtLr3

Counts
keV

(d)

O K
Si K
Ag L
Pt M

50 nm

| Element | (keV) | Mass% | Counts | Sigma | Atom% |
|---|---|---|---|---|---|
| O K | 0.525 | 16.90 | 769.14 | 1.00 | 52.38 |
| Si K | 1.739 | 8.42 | 690.24 | 0.73 | 14.86 |
| Ag L (Ref.) | 2.984 | 67.03 | 1477.64 | 2.99 | 30.81 |
| Pt M | 2.048 | 7.65 | 164.72 | 1.18 | 1.94 |
| Total | | 100.00 | | | 100.00 |

AgPt/SiO$_2$ @700 °C

OKa, AgMz, SiKa, PtMa, PtMb, PtMr, PtMl, AgLa, AgLb, AgLb2, PtLl, PtLa

Counts
keV

(e)

O K
Si K
Ag L
Pt M

50 nm

| Element | (keV) | Mass% | Counts | Sigma | Atom% |
|---|---|---|---|---|---|
| O K (Ref.) | 0.525 | 35.29 | 23106.12 | 0.38 | 62.38 |
| Si K ! | 1.739 | 30.32 | 21163.69 | 0.47 | 30.53 |
| Ag L | 2.984 | 17.97 | 5697.66 | 0.41 | 4.71 |
| Pt M | 2.048 | 16.42 | 5088.19 | 0.44 | 2.38 |
| Total | | 100.00 | | | 100.00 |

AgPt/SiO$_2$ @700 °C

OKa, AgMz, SiKa, PtMa, PtMb, PtMr, PtMl, AgLa, AgLb, AgLb2, PtLl, PtLa, PtLb, PtLb2, PtLr, PtLr3
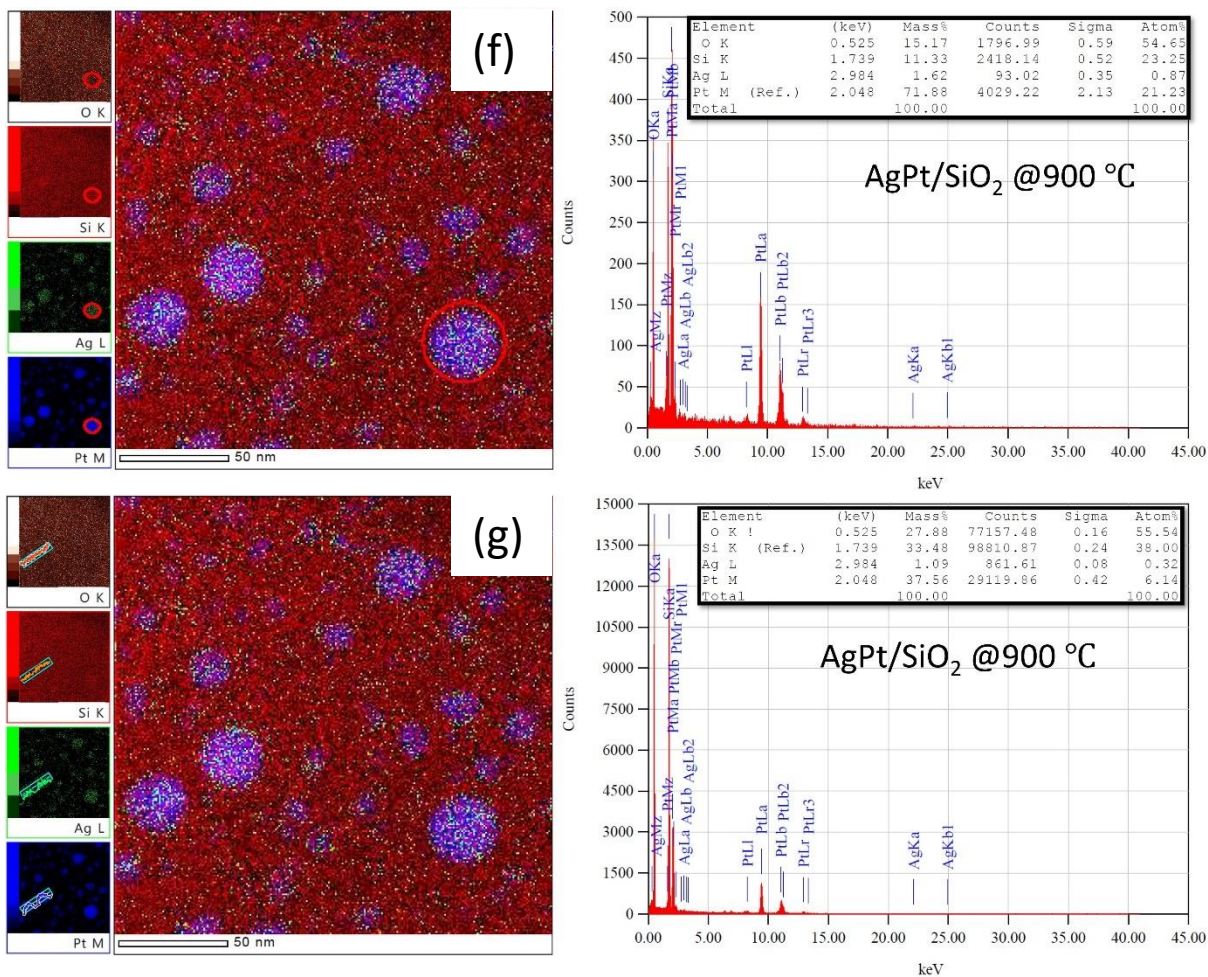
Counts
keV

**Figure S5.** (a) STEM-EDS maps of AgPt/SiO₂ at various annealing temperatures, indicated in the respective image. The bar scale of all the images are same as shown in image (a), i.e. 50 nm. Here, Ag and Pt presence is shown by green and blue colors respectively.

**(ii) High resolution TEM images:** HRTEM images were acquired after annealing at different temperatures to evaluate the thermal stability of lattice fringes (structural stability) of AgPt/SiO$_2$. It can be seen for as-deposited sample that majority of the NPs are having single domain crystal structure (i.e. all the lattice fringes are aligned in one particular orientation) and d spacing is calculated as ~0.23 nm. Interestingly, the d spacing remains unchanged and single domain structure is sustained over the entire range of annealing temperature, upto 800 ℃. These results show the structural stability of embedded NPs upon thermal annealing upto 800 ℃. Similar, single domain crystal structure is also been observed in our previous report of AuAg/SiO$_2$. However, due to the similar lattice parameters of Ag, Pt and Au, the structural stability cannot be confirmed with surety.
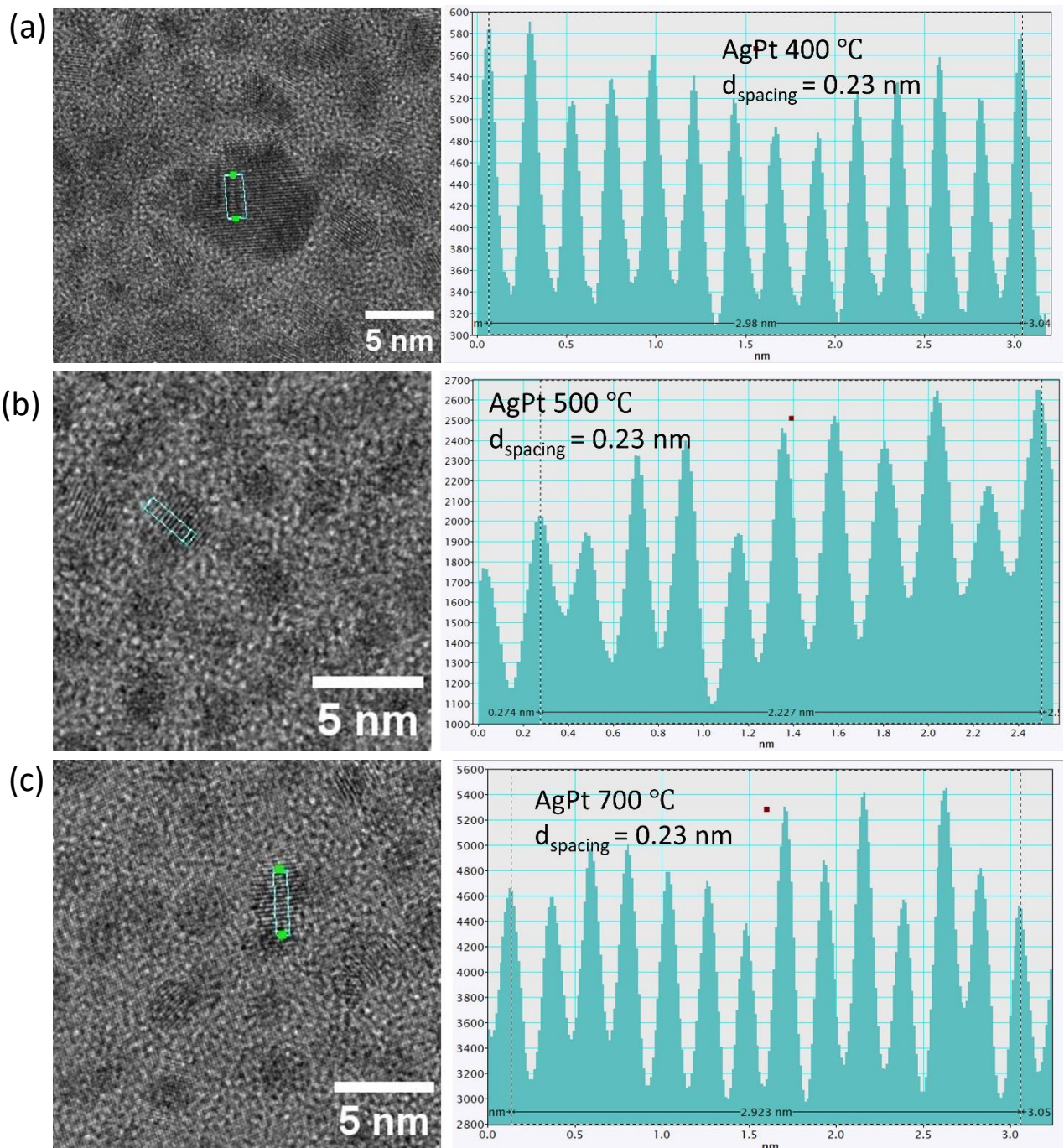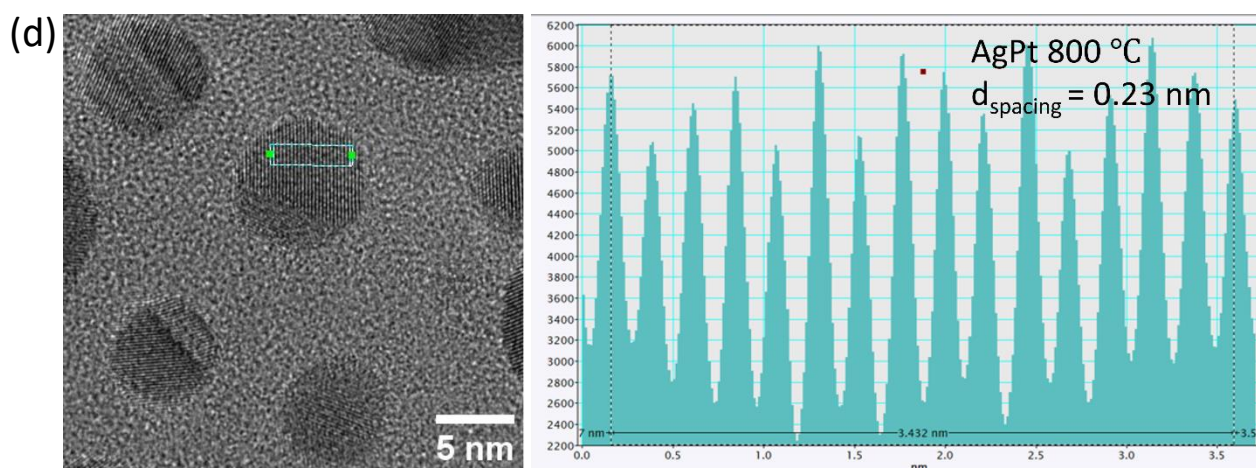
**Figure S6.** Magnified HRTEM image of AgPt/SiO$_2$ NC after annealing at different temperatures with well-defined lattice fringes of AgPt NPs (the estimated d$_{spacing}$ and annealing temperature is shown in the image itself). Line profile is also shown alongside. The scale bar of 5 nm is used for all the HRTEM images.

**References:**

1) H. Jatav, M. Shabaninezhad, M. Micetic, A. Chakravorty, A. Mishra, M. Schwartzkopf, A. Chumakov, S. V. Roth and D. Kabiraj, *Langmuir*, 2022, 38, 11983–11993.
2) L. R. Doolittle, *Nucl. Instru. Metho. in Phy. Res. Sec. B: Beam Interac. with Mat. and Atoms*, 1985, 9, 344–351.
3) G. Benecke, W. Wagermaier, C. Li, M. Schwartzkopf, G. Flucke, R. Hoerth, I. Zizak, M. Burghammer, E. Metwalli, P. Müller-Buschbaum, and M. Trebbin, *Journal of applied crystallography*, 2014, *47*(5), pp.1797-1803.
4) M. Schwartzkopf, A. Buffet, V. Körstgens, E. Metwalli, K. Schlage, G. Benecke, J. Perlich, M. Rawolle, A. Rothkirch, B. Heidmann, et al., *Nanoscale* 2013, 5, 11 5053.
5) H. Murthy, T. Zeleke, C. Ravikumar, M. Kumar, H. Nagaswarupa, *Materials Research Express.* 2020 May 20;7(5):055016.